Nat. Hazards Earth Syst. Sci. Discuss., 1, 5365–5402, 2013
www.nat-hazards-earth-syst-sci-discuss.net/1/5365/2013/
doi:10.5194/nhessd-1-5365-2013


Natural Hazards and Earth System Sciences
Open Access
Discussions



# Subsidence activity maps derived from DInSAR data: Orihuela case study

**M. P. Sanabria[1,3], C. Guardiola-Albert[2], R. Tomás[3,4], G. Herrera[2,3], A. Prieto[1], H. Sánchez[1], and S. Tessitore[2,5]**

[1]Geohazards InSAR laboratory and Modelling group, Infrastructures and services Department, Geological Survey of Spain, Rios Rosas 23, 28003 Madrid, Spain
[2]Geohazards InSAR laboratory and Modelling group, Geosciences Department, Geological Survey of Spain, Alenza 1, 28003 Madrid, Spain
[3]Unidad Asociada de investigación IGME-UA de movimientos del terreno mediante interferometría radar (UNIRAD), Universidad de Alicante, P.O. Box 99, 03080 Alicante, Spain
[4]Department of Civil Engineering, Escuela Politécnica Superior, Universidad de Alicante, P.O. Box 99, 03080 Alicante, Spain
[5]Department of Earth Sciences, Environment and Resources, Federico II University of Naples, Naples, Italy

Received: 11 September 2013 – Accepted: 13 September 2013 – Published: 8 October 2013

Correspondence to: M. P. Sanabria (m.sanabria@igme.es)

Published by Copernicus Publications on behalf of the European Geosciences Union.







## Abstract

A new methodology is proposed to produce subsidence activity maps based on the geostatistical analysis of persistent scatterer interferometry (PSI) data. PSI displacement measurements are interpolated based on Conditional Gaussian Simulation (CGS) to calculate multiple equiprobable realizations of subsidence. The result from this process is a series of interpolated subsidence values, with an estimation of the spatial uncertainty and a confidence level on the interpolation. These maps complement the PSI displacement map, improving the identification of wide subsiding areas at regional scale. At local scale, they can be used to identify buildings susceptible to suffer subsidence related damages. In order to do so, it is necessary to calculate the maximum differential settlement and the maximum angular distortion for each building of the study area. Based on PSI derived parameters those buildings in which serviceability limit state has been exceeded, and where in situ forensic analysis should be made, can be automatically identified. This methodology has been tested in Orihuela City (SE Spain) for the study of historical buildings, damaged during the last two decades by subsidence due to aquifer overexploitation.

## 1 Introduction

Subsidence caused by water withdrawal is a well-known phenomenon which affects worldwide areas. Structures built on these areas must withstand these vertical (and sometimes also horizontal) ground displacements, resulting in widespread damages when they cannot support differential settlements under their foundations. Thus the monitoring of the displacements affecting these structures plays an essential role on its serviceability and, exceptionally, on its safety. Classical surveying techniques (e.g. topographical techniques) are commonly used for monitoring structures placed on subsiding areas. However, during the last decades, Differential SAR Interferometry (DInSAR) has become an alternative method for measuring infrastructures displacements





NHESSD

1, 5365–5402, 2013



showing a good capability for measuring ground surface displacements over wide areas (Tomás et al., 2013).

Initial single interferogram DInSAR techniques (Massonnet et al., 1993; Peltzer and Rosen, 1995) evolved to advanced DINSAR techniques (A-DInSAR), which provide information on the temporal evolution of the ground displacement (Arnaud et al., 2003; Berardino et al., 2002; Ferretti et al., 2001; Mora et al., 2003; Prati et al., 2010). These techniques have been validated for subsidence monitoring with measurements obtained by classical survey techniques (Herrera et al., 2009a, b; Hung et al., 2011; Raucoules et al., 2009). These authors computed $\pm 1\,\mathrm{mm\,yr^{-1}}$ and $\pm 5$ mm errors for average displacement rate and cumulated displacements values along the Line of Sight (LOS) respectively.

Mostly, A-DInSAR techniques have been applied to monitor wide areas affected by ground surface movements associated with groundwater changes (e.g., Galloway et al., 2007; Heleno et al., 2011; Raspini et al., 2012; Stramondo et al., 2008; Tomás et al., 2010, 2011). Fewer works use these techniques to monitor singular urban structures and infrastructures and indicate its usefulness as a prevention tool (Karila et al., 2005; Bru et al., 2010; Herrera et al., 2010; Cigna et al., 2011; Sousa et al., 2013). Some authors (Cascini et al., 2007; Tomás et al., 2012) go further, and apply geotechnical criteria to A-DInsar techniques in order to identify buildings where settlement induced damages could occur.

This work focuses on the utility of A-DInSAR techniques to monitor and characterize the phenomenon of subsidence both regionally and locally, adopting a geotechnical approach for the local scale. The ground surface settlements, caused by groundwater withdrawals, of Orihuela city are evaluated by ERS-1/2 and ENVISAT ASAR sensors covering two different periods July 1995–December 2005 and January 2004–December 2008. The A-DInSAR displacement data obtained are interpolated based on Conditional Gaussian Simulation (CGS) to generate subsidence activity maps both at regional and local scale. The CGS interpolation allows quantifying the spatial uncertainty and provides a confidence level on the interpolation. From the interpolated





NHESSD
1, 5365–5402, 2013



maps, the serviceability limit states of the heritage buildings (XVI to XIX century) of the city of Orihuela (Fig. 1) are studied by means of geometrical-geotechnical criteria (i.e. differential settlements and angular distortions). Finally, a comparison of the obtained maps and individual building serviceability parameters are performed for some historical buildings which have undergone repairs in recent years.

## 2 Methodology

In this section a new proposed methodology to obtain subsidence activity maps from PSI displacement estimates is described. SAR images covering two different periods from July 1995 to December 2005 and from January 2004 to December 2008 have been processed using Stable Point Network (SPN) algorithm in order to compute PSI displacement estimates (PS).

In the first stage, a spatial analysis is performed between the PS and the available geo-thematic layers in order to determine which variables should be considered in the interpolation (Fig. 2). In this case study, these layers consist on the lithological map and the soft soil thickness map. The results of the spatial analysis reveal the existence of two different PS populations within the outcropping bedrock and the basin filling. On the other hand no direct correlation was found with the soft soil thickness.

Next step consists on the interpolation of the normalized cumulative displacement along the satellite Line of Sight (LOS) taking into account previously identified PS populations (Fig. 2). For each of them, the experimental variograms and fitted models (Goovaerts, 1997) are analysed. The parameters of the variogram models are used as input for the Conditional Sequential Gaussian Simulation (SGS) (Gómez-Hernández et al., 1993). This interpolation method generates multiple equiprobable surfaces of the displacement reproducing the observed data at their locations. The retrieved percentile maps (mean, variance, 68th percentile and 95th percentile) are analysed to generate the subsidence activity map (Fig. 2). The subsidence activity map consists





NHESSD
1, 5365–5402, 2013



of a subsidence interpolated value with a confidence level on the interpolation and estimate of the spatial uncertainty for every unsampled pixel (PS).

In the third step (Fig. 2) subsidence activity map are used to identify buildings that can be damaged by ground subsidence, according to the serviceability limit state criterion (SLS). The presence of damages mainly depends on the structure typology and the settlements magnitude and distribution. SLS are those conditions that make the structure unsuitable for its projected use. In foundations design, the most common serviceability limit states are differential settlements ($\delta_s$) and angular distortions ($\beta_{max}$), which must be less or equal than the corresponding limiting value stated for them. In the proposed case study maximum differential settlements and angular distortions are calculated for each historical building of Orihuela city based on the previously generated subsidence activity maps.

## 3 Description of the study area

The city of Orihuela is located in the Vega Baja of the Segura River (VBSR) (province of Alicante, SE Spain). The basin is filled by Neogene–Quaternary sediments deposited by the Segura River. The substratum of the VBSR basin (Fig. 1a) consists on Permo-Triassic rocks and Tertiary sediments that outcrop in the north and south of the basin (Boer et al., 1982). These materials constitute the geotechnical substratum of Orihuela City, being the Pleistocene to Holocene sediments the most compressible ones. The spatial distribution of soft soils in the VBSR increases towards to the centre of the valley reaching a maximum thickness up to 50 m (Delgado et al., 2000). These data have been digitized and completed with the geotechnical information derived from new boreholes located at the west of Orihuela city and interpolated by krigging method (Matheron, 1963) to generate the soft soil thickness map (Fig. 3). Tomas et al. (2010) characterized these soft sediments as sediments with moderate to high compressibility, exhibiting compression indexes (Cc) varying from 0.07 to 0.29 and with an average value of 0.18.





NHESSD
1, 5365–5402, 2013



From a hydrogeological point of view the study area belongs to the Guadalentín–Segura aquifer system (IGME, 1986), which is divided in two units. The first one is an unconfined shallow aquifer with low conductivity (sand, silts and clays) with the water table a few meters below the ground surface. The deep aquifer is formed by gravels, usually interbedded with marls, showing a greater hydraulic conductivity than the upper aquifer (IGME, 1986).

In the past decades, recent subsidence phenomenon in the city of Orihuela is related to the excessive water pumping from the shallow and deeper aquifer during drought periods: 1993–1996 and 2006–2008 (Tomas et al., 2010). During these periods ground water extraction in authorized and illegal drought-wells increased while groundwater recharges were reduced due to low precipitations. This groundwater withdrawal caused an important piezometric level drop (Fig. 1b) that entailed an important soil consolidation due to pore water pressure decrease (Mulas et al., 2003; Tomás et al., 2007a, b; 2010), producing moderate damages to structures and infrastructures (Martínez et al., 2004) in the whole Segura River Basin. Subsidence related damages were reported in the western part of Orihuela city in 1995 by the local press. Furthermore, several heritage buildings affected by settlements have been repaired since 90s (Louis, 2005; Maciá, 2005; Louis et al., 2012). Recently, a subsidence damage assessment of a gothic church in Orihuela City, using advanced differential interferometry for the 1995–2008 period and field data, was performed by Tomás et al. (2012).

## 4 PSI data and results

Ground subsidence measurements were obtained using a PSI technique called the Stable Point Network (SPN). A more detailed description of the PSI techniques can be found in Arnaud et al. (2003) and Duro et al. (2005). Sansosti et al. (2010) and Tomas et al. (2013) also present a review of PSI applications for subsidence research. The SPN software (Arnaud et al., 2003; Duro et al., 2005) uses the DIAPASON interferometric algorithm for all SAR data handling, e.g. co-registration task and interferogram





NHESSD
1, 5365–5402, 2013



generation. The SPN procedure generates three main products starting from a set of Single Look Complex (SLC) SAR images: (a) the average deformation velocity along the line of sight (LOS) of a single Persistent Scatterer (PS); (b) a map of height error; and (c) the LOS displacement time series of individual PS.

The SPN algorithm has been applied to C-band images acquired by the European Space Agency (ESA) ERS-1/2 and ENVISAT ASAR sensors covering two different periods July 1995–December 2005 and January 2004–December 2008. A similar crop of about 20 × 8 km was selected from the 100 × 100 km acquired SAR images, corresponding to the westernmost sector of the Vega Baja of the Segura River (Fig. 3). Each interferometric pair has been selected with a perpendicular spatial baseline smaller than 800 m, a temporal baseline shorter than 6 yr in the case of 1995–2005 and 3 yr in the case of 2004–2008, and a relative Doppler centroid difference below 400 Hz. The Digital Elevation Model (DEM) of the Shuttle Radar Topography Mission (SRTM) has been used. The PS selection for the estimation of displacements was based on a combination of several quality parameters including low amplitude standard deviation and high model coherence.

The SPN technique permitted to detect a total amount of 5730 and 4922 PS within the City of Orihuela (280 $km^2$ area) for both analysed periods (Table 1). Cumulated subsidence values vary between −119 mm and +67 mm (Fig. 3). Note that a negative value means greater subsidence and a positive value means ground surface uplift. According to the validation experiment performed by Herrera et al. (2009 a, b), the SPN error to measure cumulated displacement is ±5 mm. Therefore we define the stability range between −5 mm and +5 mm of cumulated displacement (Fig. 3).

The comparison of subsidence displacement rates reveals that subsidence displacement rates for the period 2004–2008 is 1.75 times faster than for the period 1995–2005 (Table 1). The statistical skewness (i.e. a measure of the degree of asymmetry in the distribution of sample data) reveals that the 2004–2008 period is asymmetric with a greater population of PS with negative displacement values (96 % of the PSs





NHESSD
1, 5365–5402, 2013



show cumulated subsidence lower than −5 mm), whereas the 1995–2005 population is symmetrical (84 % of the PSs showing cumulated subsidence lower than −5 mm).

## 5 Spatial analysis

In order to discriminate if the geology is a factor to be considered for the DInSAR data interpolation, the PS data were classified in two different ways and then compared one to each other. The first one separates each period of PS in two normal populations (1st and 2nd components in Fig. 4) using R software (R Development Core Team, 2010). The second separates the PS located within the alluvial sediments (Holocene) and those located on the rock outcrops (Tertiary and Permo-Triasic) forming the edge of the basin (Fig. 4). In the period 1995–2005 the PS cannot be separated into two different populations attending to the component analysis (Fig. 4a), being the stable PS heterogeneously distributed over the study area. On the contrary, in the period 2004–2008 two different normal populations can be separated (Fig. 4b) from the component analysis. The first component encloses stable PS on the stable rock outcrops, while the second component includes active PS on the younger and more compressible alluvial sediments. Consequently, through this analysis it is demonstrated that the geology is a subsidence conditioning factor, and therefore it must be taken into account to perform PS data interpolations.

Tomás et al., 2010 pointed out that the thickness of alluvial soft sediments is an important subsidence conditioning factor. In order to analyse if soft soil thickness should be considered for the interpolation the Pearson correlation coefficient ($r$) was calculated between the displacements and the thickness of soft soils. For this purpose the elaborated soft soil thickness map described in Sect. 3 was used. Note that the PSs not included within this map were not considered. The Pearson correlation coefficient ($r$) is −0.22 and −0.52 for the periods 1995–2005 and 2004–2008, respectively. Thus, it can be concluded that displacement magnitude and soft soil thickness are not directly correlated. Therefore the thickness of the soft soils cannot be considered as an additional





NHESSD
1, 5365–5402, 2013



source of information for improving the displacement data interpolation. Although this fact is apparently contradictory to the results published by Tomás et al. (2010), the observed lack of correlation can be explained considering that the piezometric level variation is also a key variable involved in the consolidation process. The soft soil thickness has a spatial variability, whereas the second one has a spatio-temporal variability.

## 6 PSI data interpolation

### 6.1 Fundamentals

Geostatistical tools are coupled with Geographic Information System (GIS) (Burrough and McDonnell, 1998) for the spatial interpolation of scattered measurements, assessing the corresponding accuracy and precision. Kriging (Matheron, 1963) is a geostatistical interpolation technique that considers both the distance and the relation between sampled data points when inferring values at unsampled locations (Journel and Huijberegts, 1978; Isaaks and Srivastava, 1989; Goovaerts, 1997). The krigging smoothing effect on the interpolated maps may be a disadvantage because the reality is expected to be more variable. As a consequence of this effect the variance of the estimated values is lower than the variance of the real values. Geostatistical simulation (Goovaerts, 1997) allows generating multiple equiprobable realizations of the attribute under study, rather than simply estimating the mean. This is a key property of this approach, since a series of realizations representing a plausible range is generated, not just one best estimate. Hence, accuracy can be estimated through distributions of inferred values at unsampled locations using the series of simulated realizations.

A large number of geostatitiscally-based algorithms exist for the simulation of realizations (i.e, Spectral Simulation, Sequential Gaussian Simulation Method, Boolean Simulation, Turning Bands, etc.). The Sequential Gaussian Simulation method (SGS) has been used in this work because of its long history and wide acceptance for environmental modelling applications. The libraries of R software (R Development Core Team,





NHESSD
1, 5365–5402, 2013



2010) Gstat (Pebesma, 2004) and geoR (Ribeiro et al., 2001), combined with SGeMS software (Remy et al., 2009) were used for the subsidence variogram visualization and analysis. One hundred equally likely realizations of subsidence were generated by SGS method using SGeMS software.

### 6.2 Variogram analysis

Variograms are widely used to quantify the spatial variability of spatial phenomena (e.g. Journel and Huijbregts, 1978; Armstrong, 1984; Olea, 1994; Goovaerts, 1997). In this work, the plot of the semivariances as a function of distance from a PS is referred to as variogram:

$$\gamma(h) = \frac{1}{2N} \sum_{i=1}^{N} [\delta(x_i) - \delta(x_i + h)]^2 \quad (1)$$

Where $N$ is the number of PS pairs separated at a distance $h$, $\delta(x_i)$ are PS cumulated displacement values and $\delta(x_i + h)$ are all the PS cumulated displacement values at a distance $h$ away from the PS $x_i$.

The analysis of this function for different separation distances ("$h$" values) allows the characterization of the spatial variability of the PSs. After the calculation of the experimental variogram, a variogram model must be inferred in order to perform the SGS. The analysis of the experimental directional variograms, lead to the detection of anisotropy (N60E), which is assumed as the maximum spatial continuity direction. The experimental and fitted variogram models obtained for the four PS populations previously defined are shown in Fig. 5 and described in Table 2. Experimental variograms for the 1995–2005 period present higher fluctuations around the sill than the ones computed for the 2004–2008 period. This behaviour can be attributed to the fact that during the period 1995–2005 the ground water level was under a recuperation phase. Hence measured subsidence rates are low and sparsely distributed and correspond to the residual consolidation of the 1992–1995 draught period. During the 2004–2008





NHESSD
1, 5365–5402, 2013



draught period there was an intensive exploitation of the aquifer in the vicinity of Orihuela City, which induced a regional subsidence over the area. This process explains the lower spatial variability of PS displacement values, which corresponds to a lower slope of the variogram models near the origin during this period. Consequently, the analyses of the variogram models confirm a different subsidence spatial variability for each period, which corresponds to different phases (piezometric level recuperation and fall) of the subsidence phenomena.

### 6.3 Subsidence activity maps generation

Subsidence activity maps are generated from the Sequential Gaussian Simulation (SGS) results. The SGS generates 100 subsidence simulations (maps). The mean of these simulations represents the expected subsidence value, which should be very similar to the result of the krigging interpolation (Figs. 6a and 7a). The spatial uncertainty is evaluated calculating the variance for the 100 performed simulations (Figs. 6b and 7b). In Orihuela City, higher variances are estimated during the 1995–2005 period than during the period 2004–2008, due to its higher spatial variability (explained in Sect. 6.2). In order to establish a confidence level for subsidence interpolated values, percentiles are calculated from 100 simulations. In our test site, 68th and 95th percentile maps are analysed for both periods (Figs. 6c, d, 7c, d). These maps display the threshold subsidence value for which there is a probability of 68 % and 95 %, respectively, that the true subsidence is greater or equal to that threshold. Note that greater subsidence means a more negative value. Visually during the period 1995–2005, 68th and 95th percentile maps are the same, being their average cumulated subsidence –17 mm. Note that the mean, which represents a 50 % confidence level, exhibits an average cumulated displacement of –36 mm that is closer to the average of the PS dataset (–47 mm). This fact suggests that the mean is the best estimator to elaborate subsidence activity maps in this period.

Concerning the period 2004–2008, 68th and 95th percentiles differ substantially from each other, visually and numerically, with an average cumulated subsidence of –47 mm





NHESSD
1, 5365–5402, 2013



and −31 mm, respectively. The latter represents very low subsidence values compared to the −47 mm average cumulated subsidence of the PSs (sampled data), which is closer to the value of the 68th percentile map. Consequently, the 68th percentile is selected to elaborate the subsidence activity map during the period 2004–2008, providing a 68 % confidence level, and the mean for the period 1995–2005 that provides a 50 % confidence level on the interpolation.

## 7 Assessment of buildings service limit state: local subsidence activity maps

### 7.1 Proposed approach

In this section a methodology is proposed to identify those buildings susceptible to suffer damages induced by subsidence. This methodology is tested in the historical buildings of Orihuela City. The proposed method consists on calculating, for each building, the maximum angular distortion ($\beta_{max}$), and the maximum differential settlement ($\delta_s$) from the subsidence activity maps previously derived (Sect. 6.3). Subsequently, these values have been compared with the allowable distortion and maximum settlement thresholds that define the serviceability limit states of the building structures. A vast number of limiting criteria for settlements and angular distortion values are available in the geotechnical literature and standards (e.g. Terzaghi and Peck, 1948; Skempton and McDonalds, 1956; Burland et al., 1977; EN 1990, 2001; CTE, 2006). In this work, considering the cohesive character of the available soils and the high rigidity of the heritage masonry building studied, we have adopted the values shown in Table 3 for angular distortion and differential settlements following the aforementioned authors' recommendations.

In order to calculate the angular distortion and the differential settlement for each historical building, a 14 m buffer is performed around each building. The buffer area is used to extract the cumulative displacement values from the subsidence activity raster maps, and represents the subsidence influence area of the building where damages





NHESSD
1, 5365–5402, 2013



can be induced. From the selected cumulative displacement values, both the maximum differential settlement ($\delta_s$) and the maximum angular distortion ($\beta_{max}$) are computed (Fig. 8).

### 7.2 Results

The results for each building indicate if the serviceability limit state is exceeded or not attending to the values of Table 3. The results of this analysis are called local subsidence maps and they are shown in Fig. 9. It is observed that the direction of the plotted vectors, both the maximum angular distortion (Fig. 9c and d) and the maximum differential settlement (Fig. 9a and b), is mainly radial to the Mesozoic reliefs and dips towards the areas of the basin where a greater thickness of compressible sediments exists.

According to retrieved results "high" damage is expected for 9 buildings in the first period and 5 in second. This is due to the more heterogeneous and variable spatial distribution of the 1995–2005 displacements, which favour the existence of greater differential settlements and angular distortion. Unfortunately, the spatial variability provides a lower confidence degree (50 %) to the SGS result, which affects to the maximum differential settlement ($\delta_s$) and the maximum angular distortion ($\beta_{max}$) calculation. On the other hand, the SGS results for the period 2004–2008 exhibit a greater confidence degree (68 %) and a more reliable calculation of the service limit state variables.

In the past two decades damages have been reported in four historical buildings (2, 13, 10 and 6 in Fig. 9): the Santo Domingo Convent (s. XVI), the San Sebastián Church (s. XV), the Royal Monastery of the Religiosas Salesas, (s. XIX) and Santas Justa and Rufina Church (s. XIV). These buildings have been studied by Louis et al. (2005, 2012), Maciá (2005) and Tomás et al. (2012). Even though the buildings damage inventory is limited for validation purposes, a double entry matrix is used to evaluate the results of the local subsidence activity maps (Table 4). True values represent reported damages on buildings. False values represent unreported damage on buildings. Positive values





NHESSD
1, 5365–5402, 2013



represent buildings with high expected damage level. Negative values represent buildings with medium to low expected damage level.

In the period 1995–2005 true positives are found in 3 of 4 buildings (75 %). The remaining true negative (25 %) was evaluated as "medium" expected damage. False positives and false negatives cannot be assessed since the damage inventory is not exhaustive. Note that minor damages could have affected several historical buildings and were not reported. However, there are 6 false positives and 17 false negative buildings. Therefore assuming that the damage inventory was exhaustive, the success of the methodology (true positives and false negatives) would represent 74 % (20 over 27 buildings). However from the buildings identified as "high" expected damage (9 positives), 3 (33 %) coincide with reported damages.

In the period 2004–2008, true positives represent 50 % (2/4), and true negatives represent 50 % (2/4), being classified as "low" expected damage. There are 3 false positives and 20 false negatives. Following the analysis presented above the methodology is successful for 81 % (22 over 27 buildings). Taking into account the positives, 2 over 5 buildings (40 %) show an expected damage that coincides with reported damages.

### 7.3 Analysis of Santa Justa and Rufina church

Santas Justa and Rufina church is located on the north bank of Segura River in the centre of Orihuela City (Figs. 1 and 10). It was declared a Spanish National Monument in 1971. During the last 20 yr damages induced by regional subsidence are affecting the structural elements of this church (Fig. 10). Tomás et al. (2012) performed a detailed analysis of the damage suffered by the building summarized here. In the 70s the principal chapel suffered an important tilt (Fig. 10). In the 90s, important settlements affected the San José chapel and the foundation was reinforced in 2002 with micropiles. In the first decade of the present century, displacements affected the whole north zone of the church and the principal chapel area. Multiple cracks where identified in the north, west, and east walls, affecting as well La Comunión cupola (Fig. 10a), the sacristy and the antesacristy (Fig. 10c). Several plaster markers were placed in the cracks in 2006





NHESSD
1, 5365–5402, 2013



and controlled in 2008 (Fig. 10b). Figure 10 shows that multiple cracks grew up during this period as a consequence of the sinking of the foundation walls caused by ground subsidence.

Subsidence activity maps, maximum differential settlement and maximum angular distortion of Santa Justa and Rufina church are shown in Fig. 11. The average cumulated displacements are −39.2 mm and −31.9 mm for 1995–2005 and 2004–2008 periods, respectively, but a greater spatial variability is appreciated for the first period. The maximum angular distortion shows medium (1995–2005) to high (2004–2008) values. Note that during the first period, the maximum angular distortion is located NE of the church, mainly affecting the main chapel. On the other hand, it is observed that during the second period the maximum angular distortion is located SW of La Comunión chapel. The orientation of the two vectors representing the maximum angular distortion is E–W, which is in agreement with the location of reported damages (Fig. 11). Concerning the maximum differential settlement, the vector direction (NE–SW) is the same for both periods. This would indicate that the church would have tilted towards the SW and as a consequence the cracks direction (normal to tension stresses) are expected to be oriented from NW to SE, coinciding with the reported damages (Fig. 11). Even if the 25 mm threshold has been not exceeded in each period, and taking into account that the direction of both vectors is similar, the combination of them both yields a 34 mm maximum differential settlement.

## 8 Discussion and conclusions

The goal of this work is to propose a novel method to produce subsidence activity maps based on the geostatistical analysis of persistent scatterer interferometry (PSI) data. These maps improve the identification and delimitation of subsiding areas at regional scale, and at local scale permit to identify buildings susceptible to suffer damages. This methodology has been tested in the city of Orihuela (SE Spain) that has been affected by subsidence induced by water extraction during the last decades.





NHESSD
1, 5365–5402, 2013



In the first stage, the statistical analysis of the PS displacement data obtained for the period 1995–2005 and 2004–2008, reveals that even though the cumulated subsidence is similar, the subsidence rate is faster in the second period than in former. This is related to the recuperation and depletion phases of the subsidence phenomena occurred along both periods.

The spatial analysis performed between the PS and the available geo-thematic layers, reveals that the geology is a conditioning factor that must be taken into account for the interpolation. This fact was proved by differentiating two normal PS populations within the outcropping bedrock and the basin filling. Also this fact was confirmed by analysing the different directional variograms where anisotropy was founded whose axis closely coincides with the axis of basin. No direct correlation has been found between PS displacement and the soft soil thickness; hence it is discarded for the interpolation.

The analysis of the variograms and the fact that the fitted models were different for each period, confirms a different subsidence spatial variability for each period, which correspond to different phases (recuperation and draught) of the subsidence phenomena. The fitted models were used to perform the Sequential Gausssian Simulation. The retrieved 100 multiple equiprobable surfaces of the displacement (mean, percentile and variance maps) were analysed to generate the subsidence activity map. This set of maps provides a subsidence interpolated surface, quantify the uncertainty of the interpolation (variance), and gives a confidence level of the interpolation (percentiles).

The regional subsidence activity map complements the PSI dataset, improving the identification and delimitation of subsiding areas at regional scale. In Orihuela city, a 68 % confidence threshold was attributed to the 2004–2008 subsidence activity map, and 50 % to that of the period 1995–2005. These maps show a lower and localized subsidence for the first period, and a greater and regionalized subsidence for the second period. Accordingly the spatial uncertainty (variance) is greater in the former period than in the later. These observations agree with the fact that during 2004–2008 there





NHESSD
1, 5365–5402, 2013



was a widespread subsidence due to water withdrawal, whereas for the period 1995–2005 a more heterogeneous subsidence is due to the groundwater level recuperation.

In the third step maximum differential settlements and angular distortions were calculated for each historical building of Orihuela city based on the previously generated subsidence activity maps. The results for each building are the local subsidence activity maps which indicate if the serviceability limit states (SLS) are exceeded, and hence damages could be produced by ground subsidence. A general overview of the maximum angular distortion and the maximum differential settlement vectors reveals that they are mainly radial to the Mesozoic reliefs and dip towards the greatest compressible sediments. Overall, from the 27 analysed historical buildings, "high" damage is expected for 9 buildings in the first period with a 50 % confidence degree, and 5 in the second period with a 68 % confidence degree.

To evaluate the results of the local subsidence activity maps a double entry matrix was used comparing the expected damage with the reported damage. For the first period the matrix shows that "high" expected damage buildings (9) coincide with reported damages in 3 of them (33 %), whereas in the second period this coincidence reaches 40 % (2/5). If we assume that the damage inventory was exhaustive, the success of the methodology (true positives and false negatives) would represent 74 % (20 over 27 buildings) for 1995–2005 period and 81 % (22 over 27 buildings) for 2004–2008 period. A detailed analysis is illustrated in Santas Justa and Rufina church, where a forensic analysis is available. Overall, the spatial and temporal locations of reported damages coincide with maximum differential settlement and maximum angular distortion vectors for both periods.

Consequently, it has been demonstrated the usefulness of the proposed methodology to generate regional and local subsidence activity maps from PSI data, providing a confidence degree on the results. These results permit to identify rapidly, subsiding areas and buildings where damages could be produced. However in situ field work and forensic analysis are necessary to confirm the targeted areas. In the next future this methodology will be tested in larger urban areas, with a larger and more detailed





NHESSD
1, 5365–5402, 2013



building damage inventory. Moreover high resolution satellite PSI displacement data will be also used to generate subsidence activity maps.

*Acknowledgements.* The authors would like to honour the memory of Enrique Chacón Oreja, Professor at the School of Mines, who sadly passed away before the publication of this article. His ideas were the inspiration of this work.

The European Space Agency (ESA) Terrafirma project has funded all the SAR data processing with the SPN technique. Additionally, this work has been partially financed by DORIS project (Ground Deformation Risk Scenarios: an Advanced Assessment Service) funded by the EC-GMES-FP7 initiative (Grant Agreement no. 242212), and the Spanish Geological and Mining Institute (IGME). This work has been also supported by the Spanish Ministry of Science and Research (MICINN) under project TEC2011-28201-C02-02 and EU FEDER.

## References

Armstrong, M.: Problems with universal kriging, J. Int. Assoc. Math. Geol., 16, 101–108, 1984.

Arnaud, A., Adam, N., Hanssen, R., Inglada, J., Duro, J., Closa, J., and Eineder, M.: ASAR ERS interferometric phase continuity Geoscience and Remote Sensing Symposium, 2003, IGARSS '03, Proceedings, 2003 IEEE International, vol. 2, 1133–1135, 21–25, doi:10.1109/IGARSS.2003.1294035, 2003.

Berardino, P., Fornaro, G., Lanari, R., and Sansosti, E.: A new algorithm for surface deformation monitoring based on small baseline differential SAR interferograms, IEEE T. Geosci. Remote, 40, 2375–2383, 2002.

Bru, G., Herrera, G., Tomás, R., Duro, J., De la Vega, R., and Mulas, J.: Control of deformation of buildings affected by subsidence using persistent scatterer interferometry, Struct. Infrastruct. Engin., 9, 188–200, doi:10.1080/15732479.2010.519710, 2010.

Burland, J. B., Broms, B. B., and de Mello, V. F.: Behaviour of foundations and structures. S. O. A. Report. IX ICSMFE, Tokyo, 2, 495–546, 1977.

Burrough, P. A. and McDonnell, R.: Principles of Geographical Information Systems, vol. 333, Oxford University Press, New York, 1998.

Cascini, L., Ferlisi, S., Peduto, D., Fornaro, G., and Manunta, M.: Analysis of a subsidence phenomenon via DInSAR data and geotechnical criteria, Ital. Geotech. J., 41, 50–67, 2007.





NHESSD

1, 5365–5402, 2013



CTE: Código Técnico de la Edificación, SE-C Seguridad structural de cimientos, 160 pp., 2006 (in spanish).
Cigna, F., Del Ventisette, C., Liguori, V., and Casagli, N.: Advanced radar-interpretation of InSAR time series for mapping and characterization of geological processes, Nat. Hazards Earth Syst. Sci., 11, 865–881, doi:10.5194/nhess-11-865-2011, 2011.
de Boer, A., Egeler, C. G., Kampschuur, W., Montenat, Ch., Rondeel, H. E., Simon, O. J., and van Winkoop, A. A.: Mapa Geológico de España, 1:50.000, IGME, Hoja 913, Orihuela, 1982.
Delgado, J., López Casado, C., Estévez, A., Giner, J., Cuenca, A., and Molina, S.: Mapping soft soils in the Segura river valley (SE Spain): a case study of microtremors as an exploration tool, J. Appl. Geophys., 45, 19–32, 2000.
Duro, J., Inglada, J., Closa, J., Adam, N., Arnaud, A.: High resolution differential interferometry using time series of ERS and ENVISAT SAR data, in: FRINGE 2003, Frascati, Italy, 1–5 December 2005.
EN 1990: 2002 Eurocode – Basis of Structural Design, CEN, 29 November 2001.
Ferretti, A., Prati, C., and Rocca, F.: Permanent scatterers in SAR interferometry, IEEE T. Geosci. Remote, 39, 8–20, 2001.
Galloway, D. and Hoffmann, J.: The application of satellite differential SAR interferometry-derived ground displacements in hydrogeology, Hydrogeol. J., 15, 133–154, doi:10.1007/s10040-006-0121-5, 2007.
Gómez-Hernández, J. J. and Journel, A. G.: Joint Sequential Simulation of MultiGaussian Fields, in: Geostatistics Tróia '92, volume 1, edited by: Soares, A., Kluwer Academic Publishers, 85–94, 1993.
Goovaerts, P.: Geostatistics for Natural Resources Evaluation, Oxford University Press, New York, 1997.
Heleno, S. I. N., Oliveira, L. G. S., Henriques, M. J., Falcão, A. P., Lima, J. N. P., Cooksley, G., Ferretti, A., Fonseca, A. M., Lobo-Ferreira, J. P., and Fonseca, J. F. B. D.: Persistent scatterers interferometry detects and measures ground subsidence in Lisbon, Remote Sens. Environ., 115, 2152–2167, doi:10.1016/j.rse.2011.04.021, 2011.
Herrera, G., Fernández, J. A., Tomás, R., Cooksley, G., and Mulas, J.: Advanced interpretation of subsidence in Murcia (SE Spain) using A-DInSAR data – modelling and validation, Nat. Hazards Earth Syst. Sci., 9, 647–661, doi:10.5194/nhess-9-647-2009, 2009a.
Herrera, G., Tomás, R., López-Sánchez, J. M., Delgado, J., Vicente, F., Mulas, J., Cooksley, G., Sánchez, M., Duro, J., Arnaud, A., Blanco, P., Duque, S., Mallorquí, J. J., Vega-Panizo, R.,





NHESSD
1, 5365–5402, 2013



and Monserrat, O.: Validation and comparison of advanced differential interferometry techniques: Murcia metropolitan area case study, ISPRS J. Photogramm., Remote Sens., 64, 501–512, 2009b.
Herrera, G., Tomás, R., Monells, D., Centolanza, G., Mallorquí, J. J., Vicente, F., Navarro, V. D., Lopez-Sanchez, J. M., Sanabria, M., Cano, M., and Mulas, J.: Analysis of subsidence using TerraSAR-X data: murcia case study, Eng. Geol., 116, 284–295, doi:10.1016/j.enggeo.2010.09.010, 2010.
Hung, W., Hwang, C., Chen, Y., Chang, C., Yen, J., Hooper, A., and Yang, J.: Surface deformation from persistent scatterers SAR interferometry and fusion with leveling data: a case study over the Choushui River Alluvial Fan, Taiwan, Remote Sens. Environ., 115, 957–967, doi:10.1016/j.rse.2010.11.007, 2011.
IGME: Calidad de Las Aguas Subterrá neas en la Cuenca Baja del Segura y Costeras de Alicante, Technical report, Instituto Geológico y Minero, Madrid, 77 pp., 1986.
Isaaks, E. H. and Srivastava, R. M.: Applied Geostatistics, Oxford University Press, New York, 1989.
Journel, A. G. and Huijbregts, Ch. J.: Mining Geostatistics, vol. 859, Academic Press, London, 1978.
Karila, K., Karjalainen, M., and Hyyppä, J.: Urban land subsidence studies in Finland using synthetic aperture radar images and coherent targets, Photogramm. J. Finland, 19, 43–53, 2005.
Louis, M.: Toma de datos y proyecto restauración Iglesia las Salesas (Orihuela), Septiembre 2005, Technical report, unpublished, 2005.
Louis, M., Spairani, Y., Huesca, J. A., and Prado, R.: La restauración de la iglesia de San Sebastián, Orihuela (Alicante). In F. C. I.p.l. C.d. P. (CICOP) (Ed.), XI Congreso Internacional de Rehabilitación del Patrimonio Arquitectónico y Edificación (pp. 202–210), Servicio de Publicaciones de la Fundación Centro Internacional para la Conservación del Patrimonio (CICOP), Cascais, Portugal, 2012.
Maciá, J. A.: Estudio diagnóstico y propuesta de intervenciones en el colegio Diocesano Santo Domingo, Technical report, unpublished, 2005.
Martínez, M., Mulas, J., Herrera, G., and Aragón, R.: Efectos de una subsidencia moderada por extracción de agua subterránea en Murcia, España, Proc. XXXIII Congress of IAH-ALHSUD, Zacatecas, Mexico, Conference on Groundwater Flow Understanding from local to regional scales, CD ROM, 2004.





NHESSD
1, 5365–5402, 2013



Massonnet, D., Rossi, M., Carmona, C., Adragna, F., Peltzer, G., Feigl, K., and Rabaute, T.: The displacement field of the Landers earthquake mapped by radar interferometry, Nature, 364, 138–142, 1993.

Matheron, G.: Principles of geostatistics, Econ. Geol., 58, 1246–1266, 1963

Mora, O., Mallorquí, J. J., and Broquetas, A.: Linear and nonlinear terrain deformation maps from a reduced set of interferometric SAR images. IEEE T. Geosci. Remote, 41, 2243–2253, 2003.

Mulas, J., Aragón, R., Martínez, M., Lambán, J., García-Arostegui, J. L., Fernández-Grillo, A. I., Hornero, J., Rodríguez, J., and Rodríguez, J. M.: Geotechnical and hydrological analysis of land subsidence in Murcia (Spain), Proc. 1st International Conference on Groundwater in Geological Engineering, 22–26 September, Bled, Slovenia, 50, 249–252, 2003.

Olea, R. A.: Fundamentals of semivariogram estimation, modeling, and usage, in: AAPG Computer Applications in Geology, edited by: Yarus, J. M. and Chambers, R. L., No. 3, Chapter 4, 27–35, 1994.

Pebesma, E. J.: Multivariable geostatistics in S: the gstat package, Comp. Geosci., 30, 683–691, 2004.

Peltzer, G. and Rosen, P.: Surface Displacement of the 17 May 1993 Eureka Valley, California, Earthquake Observed by SAR Interferometry, Science, 268, 1333–1336, doi:10.1126/science.268.5215.1333, 1995.

Prati, C., Ferretti, A., and Perissin, D.: Recent advances on surface ground deformation measurement by means of repeated spaceborne SAR observations, J. Geodyn., 49, 161–170, doi:10.1016/j.jog.2009.10.011, 2010.

Raucoules, D., Bourgine, B., De Michele, M., Le Cozannet, G., Closset, L., Bremmer, C.,Veldkamp, H., Tragheim, D., Bateson, L., Crosetto, M., Agudo, M., and Engdahl, M.: Validation and Intercomparison of Persistent Scatterers Interferometry: PSIC4 project results, J. Appl. Geophys., 68, 335–347, doi:10.1016/j.jappgeo.2009.02.003, 2009.

Raspini, F., Cigna, F., and Moretti, S.: Multi-temporal mapping of land subsidence at basin scale exploiting persistent scatterer interferometry: case study of Gioia Tauro plain (Italy), J. Map., 8, 1–11, doi:10.1080/17445647.2012.743440, 2012.

R Development Core Team: R: A language and environment for statistical computing. R Foundation for Statistical Computing, Vienna, Austria, ISBN 3-900051-07-0, available at: http://www.R-project.org (last access: 1 October 2013), 2010.





NHESSD

1, 5365–5402, 2013



Remy, N., Boucher, A., and Wu, J.: Applied Geostatistics with SGeMS: a User's Guide, Cambridge University Press, Cambridge, UK, 2009.

Ribeiro Jr, P. J. and Peter, J.: Diggle geoR: a package for geostatistical analysis R-NEWS, 1, 15–18, 2001.

Sansosti, E., Casu, F., Manzo, M., and Lanari, R.: Space-borne radar interferometry techniques for the generation of deformation time series: an advanced tool for Earth's surface displacement analysis, Geophys. Res. Lett., 37, L20305, doi:10.1029/2010GL044379, 2010.

Skempton, A. W. and McDonalds, D. H.: Allowable settlements of buildings, Proc. ICE London, 5, 727–768, 1956.

Sousa, J. J. and Bastos, L.: Multi-temporal SAR interferometry reveals acceleration of bridge sinking before collapse, Nat. Hazards Earth Syst. Sci., 13, 659–667, doi:10.5194/nhess-13-659-2013, 2013.

Stramondo, S., Bozzano, F., Marra, F., Wegmuller, U., Cinti, F. R., Moro, M., and Saroli, M.: Subsidence induced by urbanization in the city of Rome detected by advanced InSAR technique and geotechnical investigations, Remote Sens. Environ., 112, 3160–3172, doi:10.1016/j.rse.2008.03.008, 2008.

Terzaghi, K., Peck, R. B.: Soil Mechanics in Engineering Practice, John Wiley and Sons, New York, 1948.

Tomás, R., Domenech, Mira, A., Cuenca, A., and Delgado, J.: Preconsolidation stress in the Vega Baja and Media areas of the River Segura (SE Spain): causes and relationship with piezometric level changes, Eng. Geol., 91, 135–151, doi:10.1016/j.enggeo.2007.01.006, 2007a.

Tomás, R., Lopez-Sanchez, J. M., Delgado, J., Vicente, F., Cuenca, A., Mallorquí, J. J., Blanco, P., and Duque, S.: DInSAR monitoring of land subsidence in Orihuela city, Spain: Comparison with geotechnical data, 2007 International Geoscience and Remote Sensing Symposium, Barcelona, 2007b.

Tomás, R., Herrera, G., Lopez-Sanchez, J. M., Vicente, F., Cuenca, A., and Mallorquí, J. J.: Study of the land subsidence in the Orihuela city (SE Spain) using PSI data: distribution, evolution and correlation with conditioning and triggering factors, Engin. Geol., 115, 105–121, doi:10.1016/j.enggeo.2010.06.004, 2010.

Tomás, R., Herrera, G., Cooksley, G., and Mulas, J.: Persistent Scatterer Interferometry subsidence data exploitation using spatial tools: the Vega Media of the Segura River Basin case study, J. Hydrol., 400, 411–428, doi:10.1016/j.jhydrol.2011.01.057, 2011.





NHESSD

1, 5365–5402, 2013



Tomás, R., García-Barba, J., Cano, M., Sanabria, M. P., Ivorra, S., Duro, J., and Herrera, G.: Subsidence damage assessment of a gothic church using differential interferometry and field data, Struct. Health Monit., 11, 751–762, doi:10.1177/1475921712451953, 2012.

Tomás, R., Romero, R., Mulas, J., Marturià, J. J., Mallorquí, J. J., Lopez-Sanchez, J. M., Herrera, G., Gutiérrez, F., González, P. J., Fernández, J., Duque, S., Concha-Dimas, A., Cocksley, G., Castañeda, C., Carrasco, D., and Blanco, P.: Radar interferometry techniques for the study of ground subsidence phenomena: a review of practical issues through cases in Spain, Environ. Earth Sci., 1866–6280, doi:10.1007/s12665-013-2422-z, 2013.





NHESSD

1, 5365–5402, 2013



**Table 1.** Descriptive measurements for both periods.

| | 1995–2005 | 2004–2008 |
|---|---|---|
| No. of PS | 5730 | 4922 |
| PS density (PS km$^{-2}$) | 20.46 | 17.58 |
| Minimum (mm) | −118.88 | −109.30 |
| Maximum (mm) | 66.78 | 12.35 |
| Mean (mm yr$^{-1}$) | −2.45 | −4.28 |
| Standard deviation (mm) | 21.14 | 13.23 |
| Skewness | −0.07 | −1.85 |





NHESSD
1, 5365–5402, 2013



**Table 2.** Parameters of the variogram models for each normalized PS data group.

| Period | Geology | Model | Nugget | Partial sill | Effective range 60° | Effective range 150° |
|---|---|---|---|---|---|---|
| 1995–2005 | Soft soils | Exponential | 0.22 | 0.76 | 3240 | 1860 |
| | Geotechnical Sustratum | Exponential | 0.15 | 0.43 | 1550 | 1300 |
| 2004–2008 | Soft soils | Spherical | 0.16 | 1.05 | 4410 | 3150 |
| | Geotechnical Sustratum | Spherical | 0.4 | 0.5 | 4620 | 3920 |





NHESSD
1, 5365–5402, 2013



**Table 3.** Adopted maximum angular distortion ($\beta_{max}$) and maximum differential settlement ($\delta_s$) for the performed analysis.

| Expected damage level | Maximum angular distortion ($\beta_{max}$) | Maximum differential settlement ($\delta_s$) |
|---|---|---|
| Low | $< 1/3000$ | $< 25$ mm |
| Medium | $1/3000$–$1/2000$ | – |
| High | $> 1/2000$ | $> 25$ mm |





NHESSD
1, 5365–5402, 2013



**Table 4.** Evaluation of local subsidence activity map for each period: double entry matrix.

| Period | Reported damage | Expected damage level | |
|---|---|---|---|
| | | Positive (high) | Negative (medium and low) |
| 1995–2005 | True (4 buildings) | 3/4 | 1/4 |
| | False (23 buildings) | 6/23 | 17/23 |
| 2004–2008 | True (4 buildings) | 2/4 | 2/4 |
| | False (23 buildings) | 3/23 | 20/23 |





NHESSD
1, 5365–5402, 2013



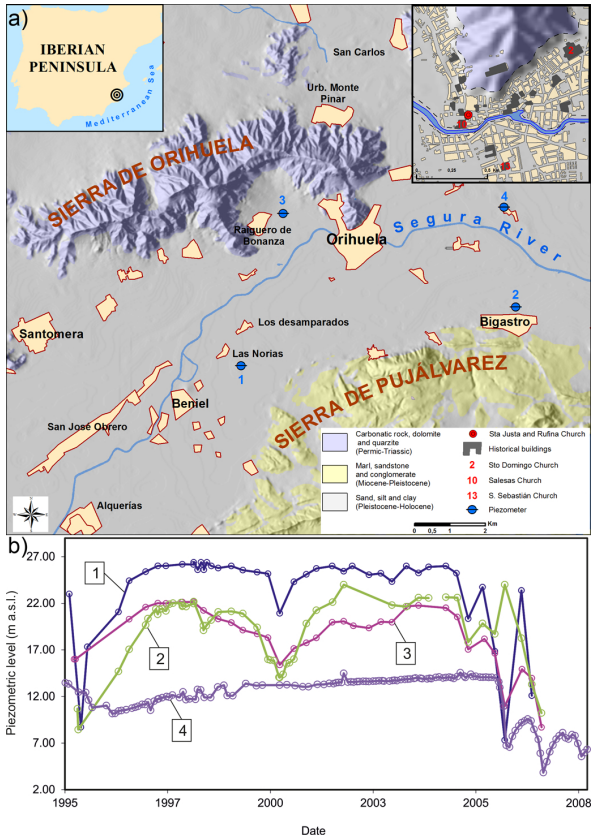


**Fig. 1. (a)** Location and geology of the study area. **(b)** Piezometric level evolution for the study period. See location of piezometers in **(a)**.





NHESSD
1, 5365–5402, 2013

Subsidence activity maps derived from DInSAR data: Orihuela case study

M. P. Sanabria et al.



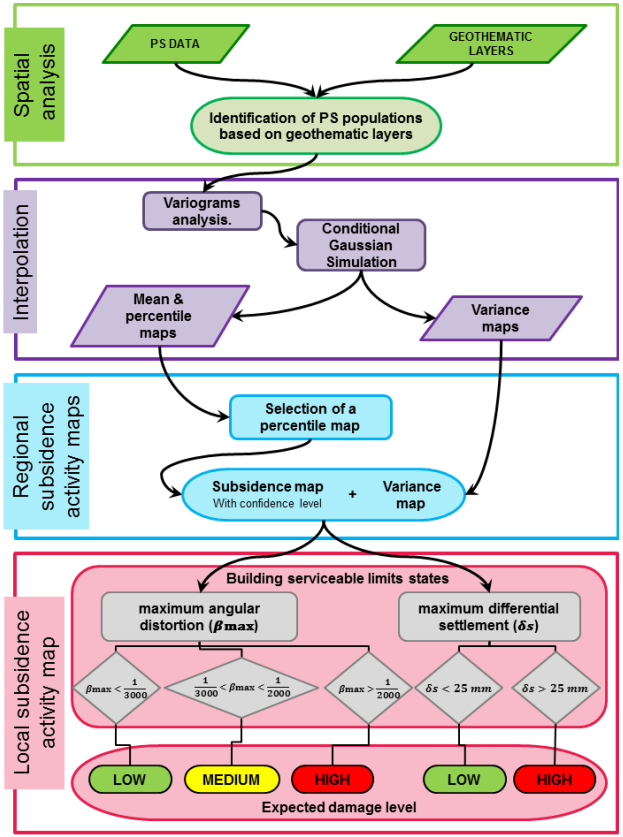


**Fig. 2.** Proposed methodology for the elaboration of subsidence activity maps.





NHESSD
1, 5365–5402, 2013

Subsidence activity maps derived from DInSAR data: Orihuela case study

M. P. Sanabria et al.



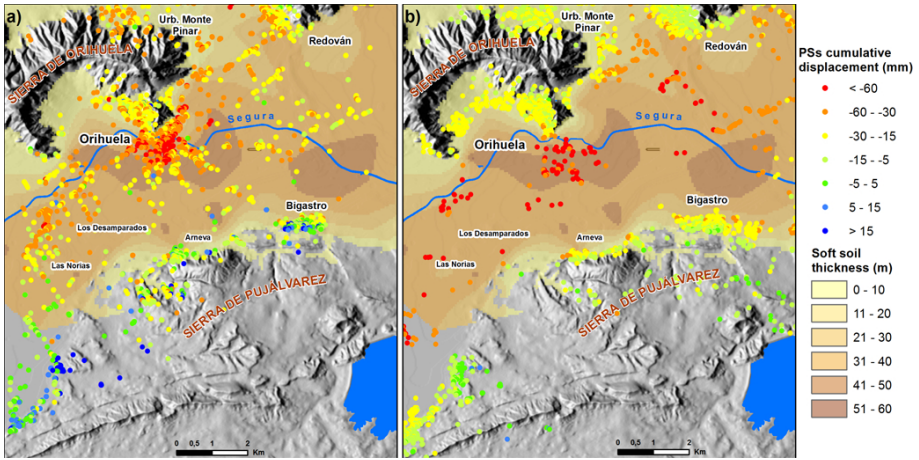


**Fig. 3.** Cumulative displacement (mm) along the LOS superimposed to soft soil thickness for both processed periods: **(a)** 1995–2005 and **(b)** 2004–2008.





NHESSD
1, 5365–5402, 2013



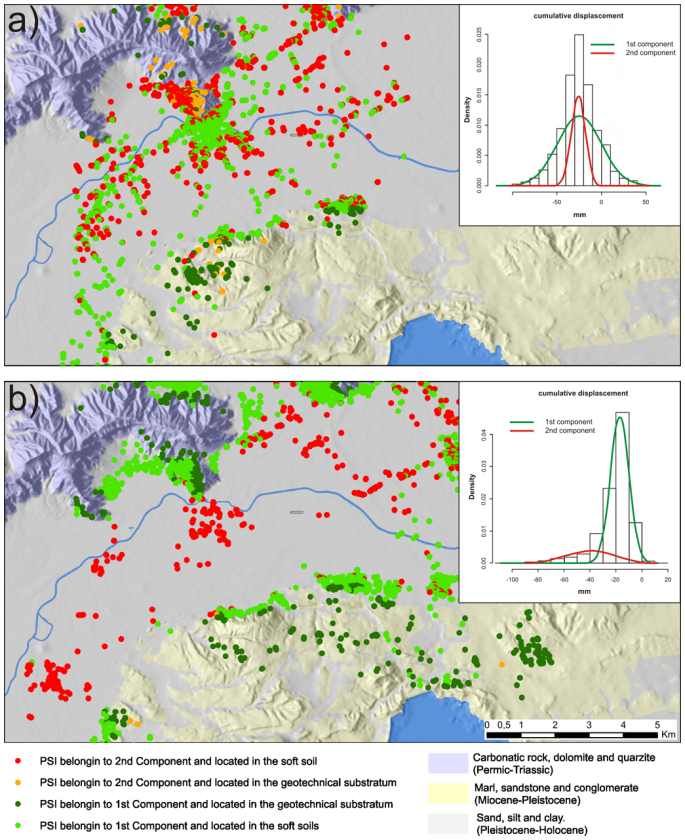


**Fig. 4.** PS classification attending to normal distributions (1st component and 2nd component) and geological criteria for both studied periods: **(a)** 1995–2005 and **(b)** 2004–2008.





NHESSD
1, 5365–5402, 2013

Subsidence activity maps derived from DInSAR data: Orihuela case study

M. P. Sanabria et al.



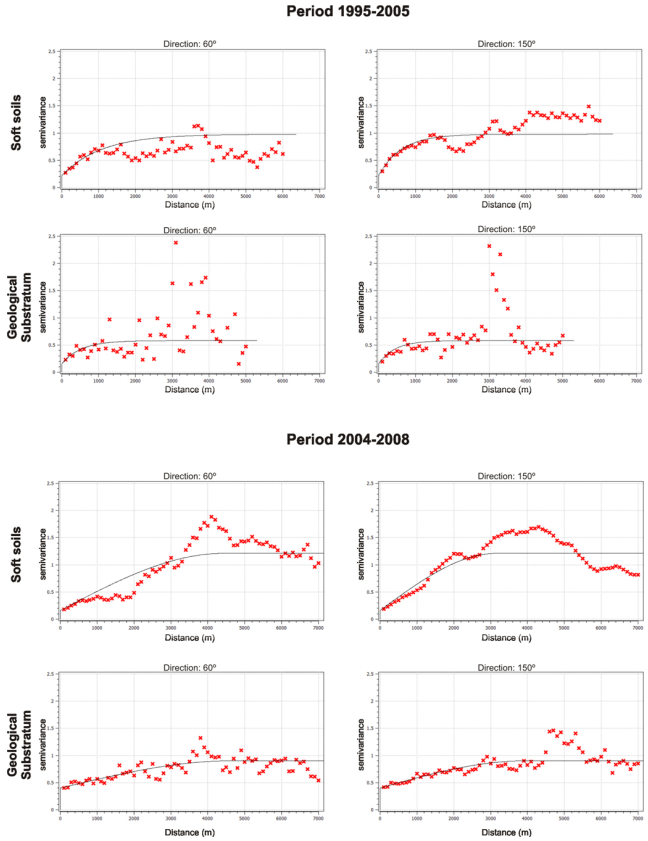


**Fig. 5.** Experimental variograms with fitted theoretical model in 60° and 150° direction (angles are counted from the North increasing clockwise).





NHESSD
1, 5365–5402, 2013

Subsidence activity maps derived from DInSAR data: Orihuela case study

M. P. Sanabria et al.



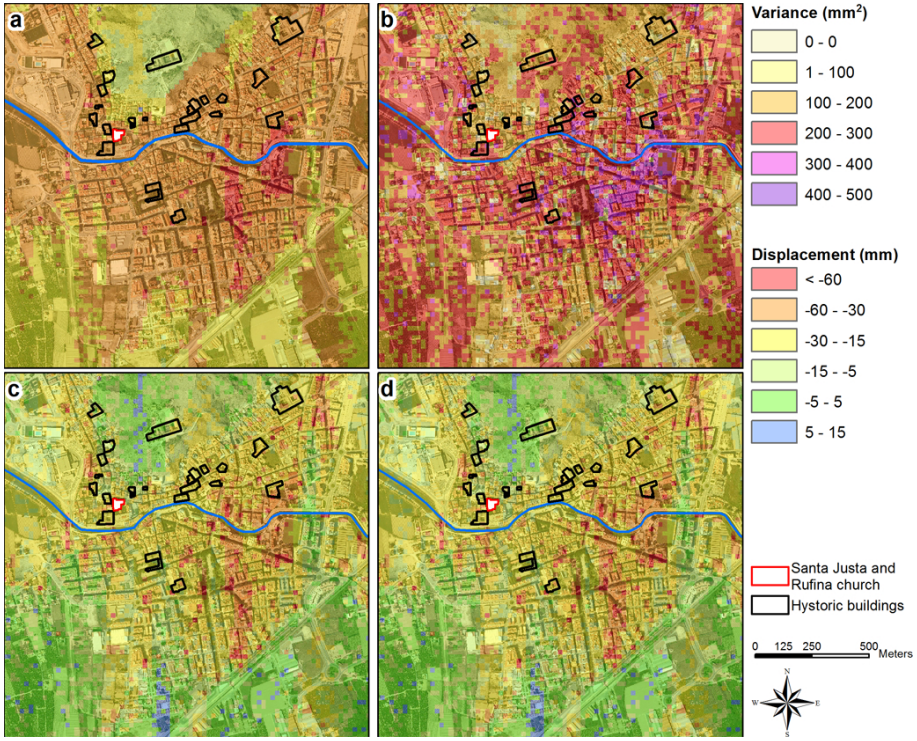


**Fig. 6.** Sequential Gaussian conditional simulations results for 1995–2005 period: **(a)** mean; **(b)** variance; **(c)** 68th percentile; and **(d)** 95th percentile.





NHESSD
1, 5365–5402, 2013



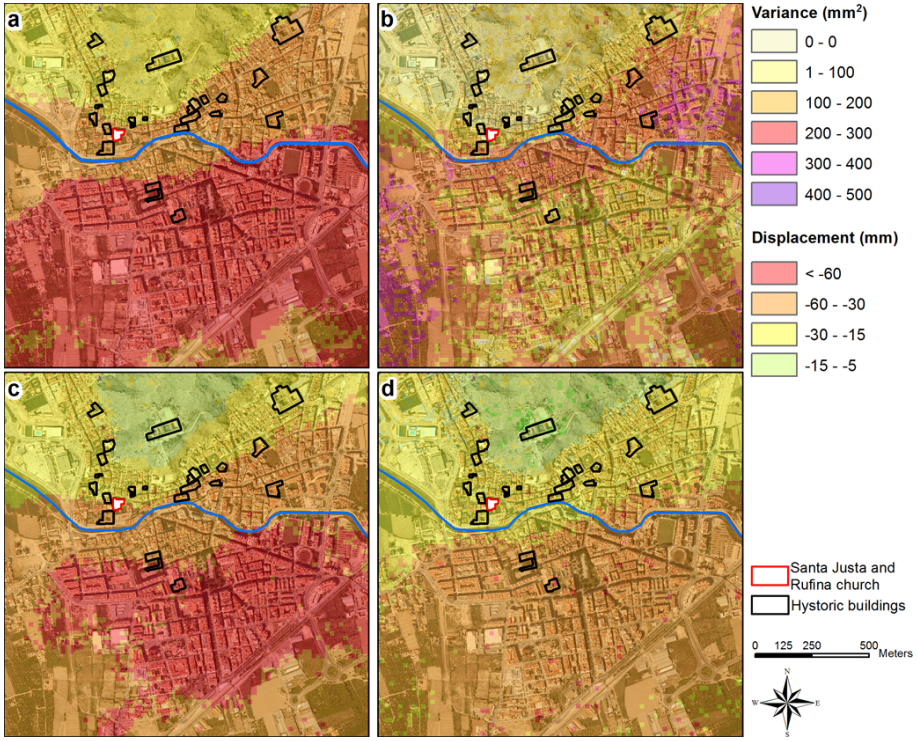


**Fig. 7.** Sequential Gaussian conditional simulations results for 2004–2008 period: **(a)** mean; **(b)** variance, **(c)** 68th percentile; and **(d)** 95th percentile.





NHESSD
1, 5365–5402, 2013



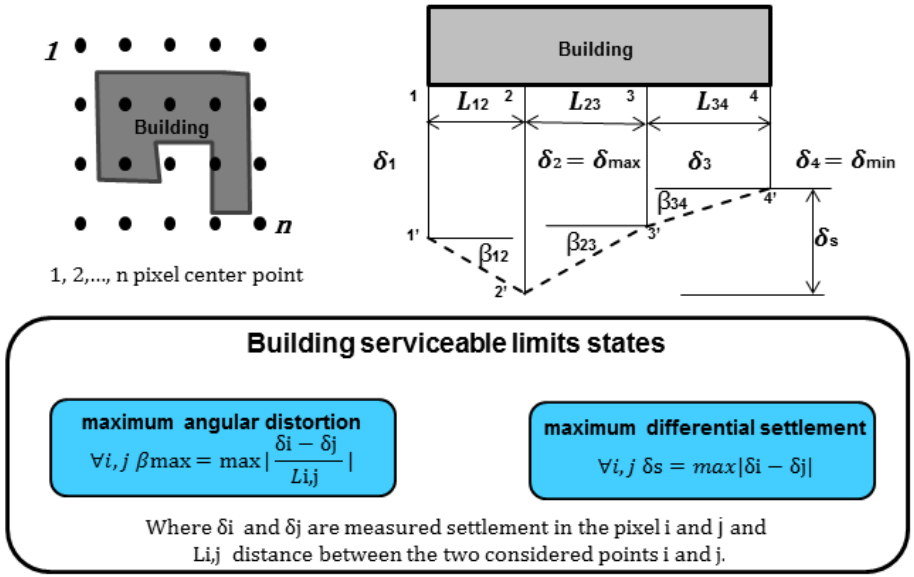


**Fig. 8.** Schema and parameters computed for serviceability limit states analysis.





NHESSD
1, 5365–5402, 2013



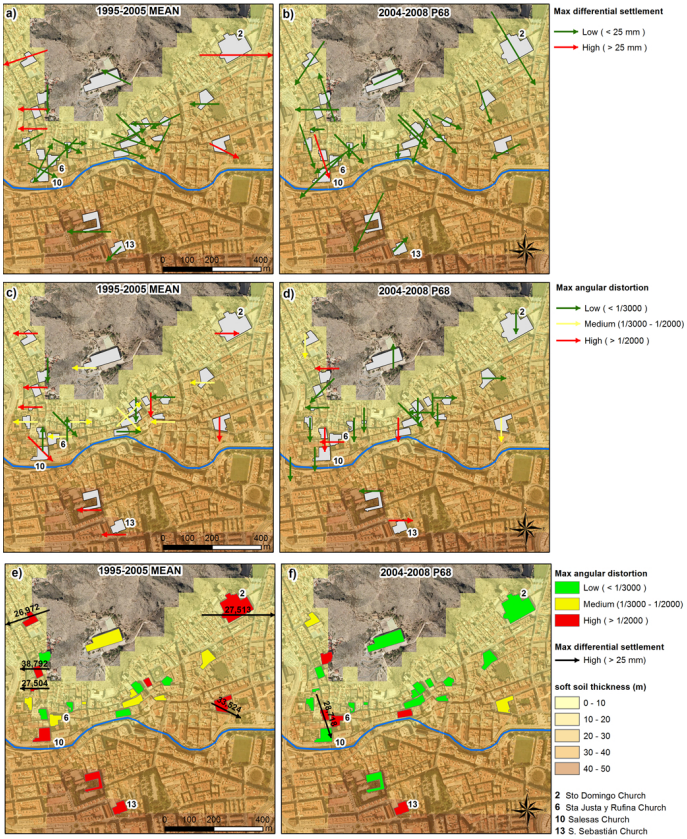


**Fig. 9.** Local subsidence activity maps for both studied periods. Notice that the used interpolation surfaces are the mean and the 68th percentile for 1995–2005 and the 2004–2008 periods respectively.





NHESSD
1, 5365–5402, 2013



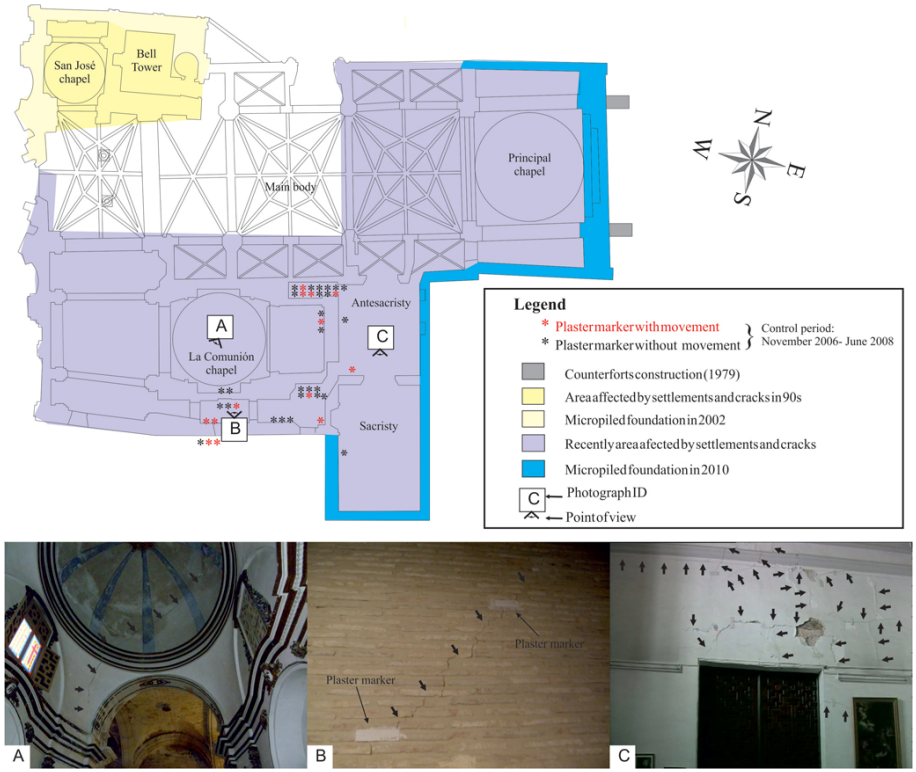


**Fig. 10.** Location of the structural damage and restoration and reinforcement actions performed on Santas Justa and Rufina church (modified from Tomás et al., 2012).





NHESSD
1, 5365–5402, 2013

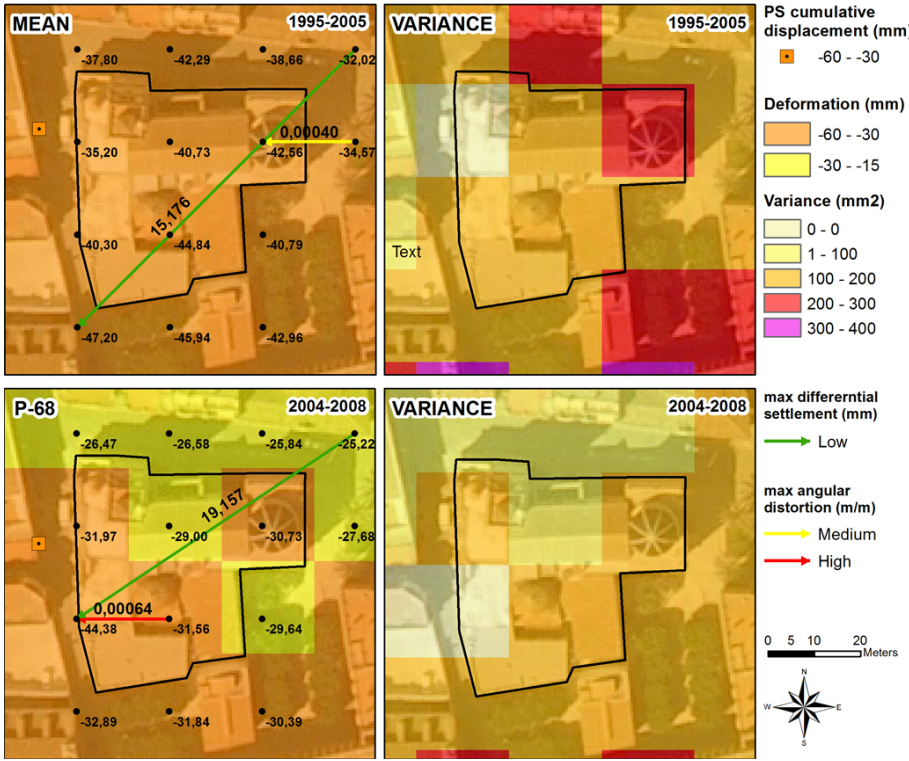


**Fig. 11.** Mean (1995–2005), 68th percentile (2004–2008) and variance for both studied periods in the vicinity of the Santas Justa and Rufina church.





NHESSD
1, 5365–5402, 2013